Review

Spectroscopy of antiprotonic helium atoms and its contribution to the fundamental physical constants

By Ryugo S. HAYANO*[1,†]

(Communicated by Toshimitsu YAMAZAKI, M.J.A.)

Abstract: Antiprotonic helium atom, a metastable neutral system consisting of an antiproton, an electron and a helium nucleus, was serendipitously discovered, and has been studied at CERN's antiproton decelerator facility. Its transition frequencies have recently been measured to nine digits of precision by laser spectroscopy. By comparing these experimental results with three-body QED calculations, the antiproton-to-electron massratio was determined as 1836.152674(5). This result contributed to the CODATA recommended values of the fundamental physical constants.

Keywords: antiproton, CERN, fundamental physical constants, laser spectroscopy

At CERN's antiproton decelerator (AD), the ASACUSA (atomic spectroscopy and collisions using slow antiprotons) collaboration, a Japan-Austria-Hungary-Italy-Denmark-Germany group led by the author, has been working on the precision laser spectroscopy of antiprotonic helium atoms since 2000.[1),2)] By comparing the measured laser transition frequencies with three-body quantum electrodynamics (QED) calculations,[3),4)] we have determined the antiproton-to-electron mass ratio $m_{\bar{p}/me}$ to the level of 2×10^{-9}.[5)] Together with the atomic transition frequencies in hydrogen and deuterium, our results (assuming CPT symmetry, i.e., the equality of particle-antiparticle masses) yield information on the Rydberg constant, the proton and deuteron charge radii, and the relative atomic mass of the electron, in the CODATA recommended values of the fundamental physical constants 2006.[6)]

In this article, we describe how a series of nuclear physics experiments ultimately led both to a more precise knowledge of the fundamental physics constants and to testing the CPT symmetry theorem.

1. History

It was in late 80's at the 12-GeV proton synchrotron at KEK, Japan, when we first discovered an intriguing anomaly. Our aim then was to search for a sigma hypernucleus ${}^{4}_{\Sigma}$He,[7)] a four-body system comprising a Σ hyperon and a three-nucleon core, produced in the ^{4}He(stopped K^-, π^-) reaction. The experiment was done by stopping kaons in a liquid helium target, and by measuring the momenta of outgoing pions using a magnetic spectrometer.

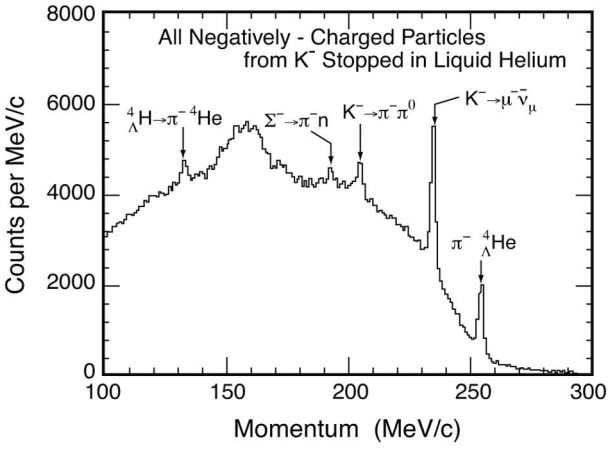

Fig. 1. Momentum spectrum of negatively charged particles emitted after K^- stopping in liquid helium. Only the K^- weak-decay peaks are visible with delayed timing selection. From ref. 8.

Figure 1 shows a momentum spectrum of negatively-charged particles measured by the magnetic spectrometer.[8)] It is in this spectrum we found the abovementioned anomaly.

*1 Department of Physics, The University of Tokyo, Tokyo, Japan.
† Correspondence should be addressed: R.S. Hayano, Department of Physics, The University of Tokyo, 7-3-1, Hongo, Bunkyo-ku, Tokyo 113-0033, Japan (e-mail: hayano@phys.s.u-tokyo.ac.jp).

doi: 10.2183/pjab.86.1

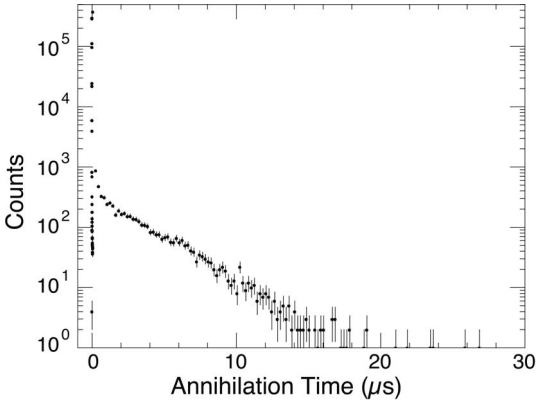

Fig. 2. The antiproton annihilation time spectrum measured by stopping antiprotons in liquid helium at KEK. From ref. 10.

The peak at 255 MeV/c is due to the formation of ${}^{4}_{\Lambda}$He hypernuclei, and the bump around 170 MeV/c corresponds to the Σ hypernuclear formation. The dominant peak at 235 MeV/c and another peak at 205 MeV/c are due respectively to $K^- \to \mu^- \overline{\nu}$ (aka $K_{\mu 2}$) and $K^- \to \pi^- \pi^0$ (aka $K_{\pi 2}$) weak decays. The observation of $K_{\mu 2}$ and $K_{\pi 2}$ peaks was totally unexpected, because the K^- cascade time, the time difference between the K^- atomic capture and the K^- nuclear absorption, is known to be quite short, (indeed as short as $\approx$ ps as is also the case for π^- and $\bar{p}$), while the kaon weak-decay lifetime is 12 ns. Thus, there is no way for the slow weak decay to compete with the fast cascade to produce such large peaks, which accounted for some 3% of the stopped K^-, unless such kaons are somehow "trapped" during the cascade process.

A natural question to ask was if similar "cascade trapping" can be observed in other exotic helium atoms. We did find a similar anomaly in the case of π^--helium,[9] but the most spectacular was the discovery of $\bar{p}$ longevity in helium.[10] Shown in Fig. 2 is the $\bar{p}$ annihilation time spectrum, i.e., the distribution of time difference between the $\bar{p}$ arrival in the target and the $\bar{p}$ annihilation. The peak at $t = 0$, containing about 97% of the events, is due to the normal, prompt annihilation. This however is followed by an anomalous delayed component. The data taken on a liquid nitrogen target just had a prompt peak. We thus serendipitously found that about 3% of antiprotons trapped in liquid helium survived with a mean lifetime of 3μs. This was the beginning of our long series of experiments on antiprotonic helium.

2. Metastability of antiprotonic helium

Normally, when an antiproton is stopped in matter, it annihilates on a nucleus within picoseconds, leaving no time for high-precision spectroscopy during any preceding atomic cascade. The above described exception is now known to occur only in helium, and has been shown to be due to the formation of the antiprotonic helium atom (hereafter denoted $\bar{p}\mathrm{He}^+$), a naturally-occurring antiproton trap in which an antiproton can be "stored" for several microseconds. This anomaly had been in fact theoretically predicted by Condo and Russell more than 40 years ago,[11),12)] but had never been observed before our work. The $\bar{p}^4\mathrm{He}^+$ atoms have the following remarkable features:

1. The atom has a metastable lifetime in excess of a microsecond. This longevity occurs when the antiproton occupies a near-circular orbit having a large $n(\sim 38)$ and also large $L(\gtrsim 35)$.
2. The $\bar{p}^4\mathrm{He}^+$ atoms can be abundantly produced just by stopping antiprotons in a helium target. Then, about 3% of the stopped antiprotons automatically become trapped in the metastable states.
3. We usually use low-temperature ($T \sim 10$ K) helium gas as the target. The $\bar{p}^4\mathrm{He}^+$ atoms that are produced collide with the surrounding helium atoms and are thermalized. Therefore, the antiprotonic helium atoms are already cold and are well suited for high-precision spectroscopy (i.e., small Doppler width).
4. We have demonstrated already that we can perform laser spectroscopy of $\bar{p}^4\mathrm{He}^+$. Note that we are not changing the electronic state as in ordinary laser spectroscopy, but are inducing transitions between different antiproton orbits.

Figure 3 shows an energy level diagram of $\bar{p}^4\mathrm{He}^+$. The levels indicated by the continuous lines have metastable ($\gtrsim 1$ μs) lifetimes and de-excite radiatively, while the levels shown by wavy lines are short lived ($\lesssim 10$ ns) and de-excite by Auger transitions to antiprotonic helium ion states (shown by dotted lines). Since the ionic states are hydrogenic, Stark collisions quickly induce antiproton annihilation on the helium nucleus, also indicated in Fig. 3.

3. Principle of $\bar{p}^4\mathrm{He}^+$ laser spectroscopy

Laser spectroscopy of $\bar{p}^4\mathrm{He}^+$ works as follows: As shown in Fig. 3, there is a boundary between metastable states and short-lived states. For exam-

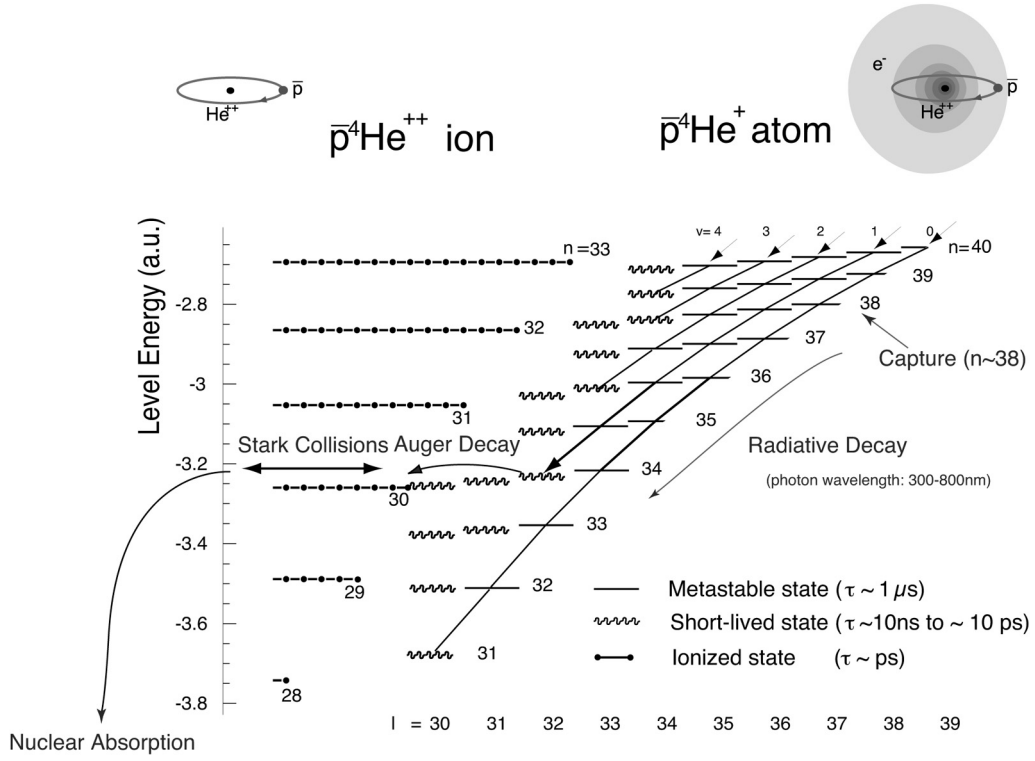

Fig. 3. Level diagram of $\bar{p}^4\mathrm{He}^+$ in relation to that of $\bar{p}^4\mathrm{He}^{++}$. The continuous and wavy bars stand for metastable and short-lived states, respectively, and the dotted lines are for L-degenerate ionized states.

ple, $(n, L) = (35, 33)$ is metastable, while $(n, L) = (34, 32)$, which can be reached from (35, 33) by an $E1$ transition, is short lived. Thus, if we use a laser ($\lambda = 372.6$ nm in this particular case) to induce a transition from $(35, 33)$ to $(34, 32)$, (and of course if an antiproton happens to be occupying the $(35, 33)$ level at the time of laser ignition), the antiproton is de-excited to the short-lived state, which then Auger decays to an ionic $(n_i, L_i) = (30, 29)$ state within $\lesssim 10$ ns. The ionic state is then promptly destroyed by Stark collisions, leading to the nuclear absorption or annihilation of the antiproton. Adding all these together, we expect to see a sharp increase in the $\bar{p}$ annihilation rate in coincidence with a resonant laser pulse, as shown in Fig. 4. We measure the intensity of the laser-induced annihilation spike as a function of laser detuning to obtain the transition frequency ν_{exp}.

The corresponding theoretical values ν_{th} are obtained by first solving a non-relativistic three-body Schrödinger equation using a complex-coordinate rotation (CCR) variational method,[23] and then perturbatively applying relativistic and quantum-electrodynamical corrections. In the coordinate system

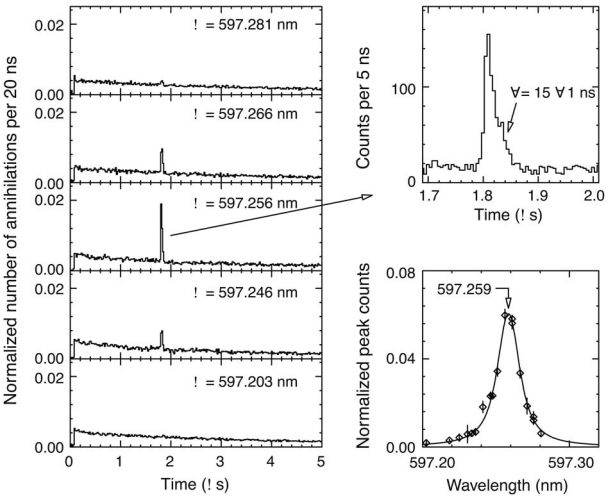

Fig. 4. Laser resonance of the $(39, 35) \rightarrow (38, 34)$ transition in $\bar{p}^4\mathrm{He}^+$. Left: Observed time spectra of delayed annihilation of antiprotons with laser irradiation of various wavelengths near 597.2 nm. Upper right: Enlarged time profile of the resonance spike. Lower right: Normalized peak count versus wavelength in the resonance region. From ref. 13.

centered on the helium nucleus (atomic base), the non-relativistic Hamiltonian in atomic units can be written as,

$$\mathcal{H} = -\frac{1}{2\mu_{12}}\nabla_1^2 - \frac{1}{2\mu_{13}}\nabla_2^2 - \frac{m_3}{m_1}\nabla_1\nabla_2 + \frac{z_1 z_2}{r_{12}} + \frac{z_1 z_3}{r_{13}} + \frac{z_2 z_3}{r_{23}} \quad [1]$$

$$\mu_{ij}^{-1} \equiv m_i^{-1} + m_j^{-1},$$

wherein the indices 1, 2 and 3 respectively correspond to He, $\bar{p}$ and e^-.

Intuitively, the transition frequency from the state (n, L) to (n', L') can be written similarly to the well-known hydrogen formula,

$$\nu(n, L \to n', L') = Rc\frac{M^*}{m_e} Z_{\rm eff}^2(n, L \to n', L')\left(\frac{1}{n^2} - \frac{1}{n'^2}\right) + QED \quad [2]$$

where R is the Rydberg constant, c is the speed of light, M^*/m_e is the reduced antiproton-to-electron mass ratio and $Z_{\rm eff}$ is the effective nuclear charge. Here, $Z_{\rm eff}$ would be 2 for the antiprotonic helium ion ($\bar{p}\mathrm{He}^{++}$), but is <2 in the case of $\bar{p}\mathrm{He}^{+}$ due to the nuclear-charge shielding by the remaining electron, and is evaluated in the three-body calculation. This shows how $m_{\bar{p}}/m_{\rm e}$ can be deduced from the precision measurement of $\nu_{\rm exp}$ with the help of three-body calculations.

4. Progress over the years

Figures 5 and 6 show our progress over the years. The first series of measurements, conducted at CERN's low energy antiproton ring (LEAR, closed down at the end of 1996) were of exploratory nature, in which we established the formation and structure of the antiprotonic helium atoms.[11] Our first successful observation of the $(n, L) = (39, 35) \to (38, 34)$ laser resonance of $\bar{p}^4\mathrm{He}^+$ at $\lambda = 597.3$ nm[13] triggered theoretical efforts to perform high-precision three-body QED calculations, which in turn helped us guide the search for new transitions.

The most important outcome of the LEAR era was the study of the density-dependent shifts and widths of the transition frequencies.[14] Since the $\bar{p}^4\mathrm{He}^+$ atoms were produced by stopping antiprotons in a helium gas target of temperature $T \approx 5$ K and pressure $P \approx 0.5$ bars, or atomic density of $\rho \approx 10^{21}$ atoms per cm^3, the atoms undergo many collisions against ordinary helium atoms, producing density-linear (as well as state-dependent) shift of the transition frequencies of ≈ 500 MHz. By taking data at several different target densities in the range 0.1–3 $\times$ 10^{21} cm^{-3}, and extrapolating to the zero target density, we were able to determine two transition frequencies of $\bar{p}^4\mathrm{He}^+$ ($(n, L) = (39, 35) \to (38, 34)$ and

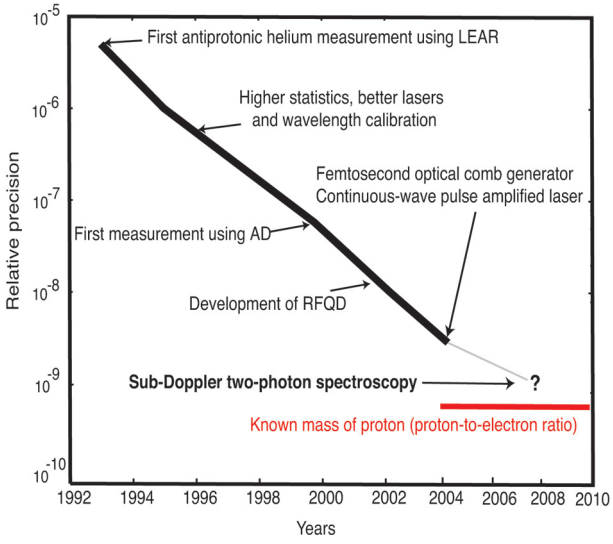

Fig. 5. Limit on the possible differences between the antiproton mass $m_{\bar{p}}$ (and charge $Q_{\bar{p}}$) and those of the proton's measured over the years, derived from $\bar{p}^4\mathrm{He}^+$ laser spectroscopy. The experimental techniques used to improve the precision are indicated.

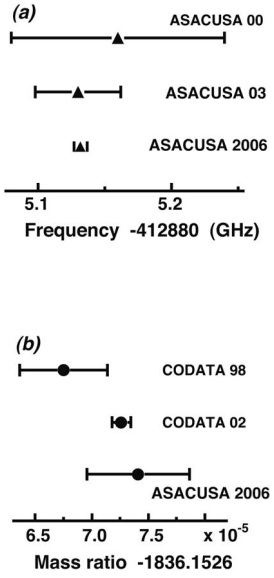

Fig. 6. (a): Frequency of the $\bar{p}^4\mathrm{He}^+$ transition $(n, L) = (37, 35) \to (38, 34)$ measured by the ASACUSA collaboration over the years. (b): m_p/m_e recommended by the CODATA98 and 2002 compilations, and $m_{\bar{p}}/m_e$.

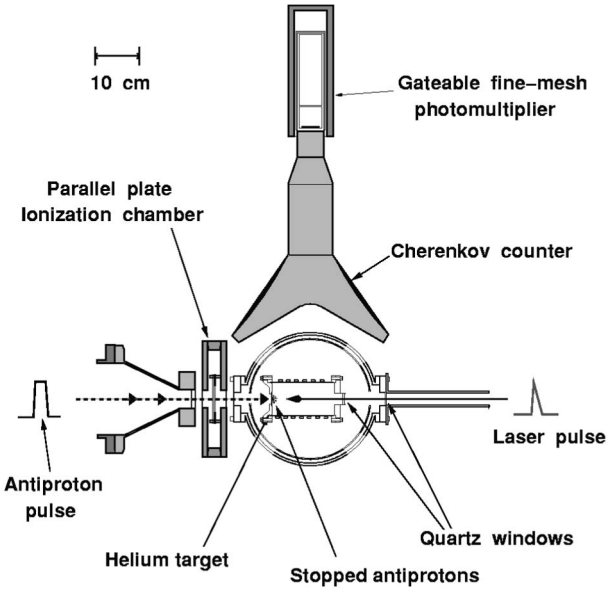

Fig. 7. Antiproton beam, helium gas target and antiproton annihilation detectors. From ref. 16.

$(37, 34) \rightarrow (36, 33)$) with precisions $\delta\nu/\nu$ of $0.5 - 1 \times 10^{-6}$.[14)]

In our first experiment at the CERN AD, we measured six transition frequencies of $\bar{p}^4\mathrm{He}^+$ to $\delta\nu/\nu = 1 - 10 \times 10^{-7}$.[15)] The essential difference between the LEAR and the AD experiments was the time structure of the antiproton beam. At LEAR, antiprotons were slowly extracted from the LEAR ring, so that laser was fired for each $\bar{p}^4\mathrm{He}^+$-candidate event which occurred randomly with a mean rate of some 300 Hz. In contrast, the AD provides a short pulse of ≈ 100-ns wide containing some 3×10^7 $\bar{p}$s, repeated every 100 s. A single laser pulse in this case irradiates some 10^6 metastable atoms. The conventional event-by-event collection of antiproton-annihilation events used at LEAR is impossible with the pulsed beam at AD. We thus developed an entirely new detection scheme (Fig. 7) based on analogue waveform (delayed-annihilation time spectra (DATS)) recording of Čerenkov counter(s) viewed by gateable photomultipliers. Here, because of the velocity-selectivity of the Čerenkov radiation, the Čerenkov counters are sensitive to the energetic pions ejected from the antiproton annihilation events. The Good control of systematic errors by stabilizing the laser frequency, intensity, the antiproton-beam position, etc., over a long measuring time of ≈ 8 hours was essential to achieve high precision.

Table 1. QED corrections to the $(39, 35) \rightarrow (38, 34)$ transition in $\bar{p}^4\mathrm{He}^{+3)}$

ΔE_{nr}	=	501 972 347.9
ΔE_{rc}	=	−27 526.1
ΔE_{a_e}	=	233.3
ΔE_{se}	=	3 818.1
ΔE_{vp}	=	−122.5
ΔE_{kin}	=	37.3
ΔE_{exch}	=	−34.7
$\Delta E^{(3)}_{recoil}$	=	0.8
$\Delta E_{two\text{-}loop}$	=	0.9
ΔE_{nuc}	=	2.4
ΔE_{α^4}	=	−2.6
ΔE_{total}	=	501 948 754.9(1.3)(0.5)

E_{nr} is the non-relativistic variational calculation result, to which all other corrections are applied perturbatively. E_{rc} is the relativistic correction to the electron, E_{a_e} is the electron's anomalous magnetic moment correction, E_{se} is the 1-loop self energy term, E_{vp} is the 1-loop vacuum polarization, E_{kin} is the relativistic correction to the heavy particles ($\bar{p}$ and helium nucleus), E_{exch} and $E^{(3)}_{recoil}$ are the first- and third-order transverse photon exchange corrections, $E_{two\text{-}loop}$ is the two-loop QED corrections, E_{nuc} is the finite nuclear-charge distribution correction, and E_{α^4} is the α^4-order QED correction.

In the first measurement at AD, the zero-density extrapolation procedure was still unavoidable (see Fig. 8), but this was largely eliminated by constructing a radio-frequency quadrupole decelerator (RFQD), an "inverse linac" which decelerates the 5.3 MeV antiprotons ejected from the AD ring to <100 keV with an efficiency of 20–25%.[17)] Using the RFQD (Fig. 9), the antiprotons can be stopped in a much lower-density target having $\rho \approx 10^{17}$ cm^{-3}. In 2003, we determined 7 transition frequencies of $\bar{p}^4\mathrm{He}^+$ and 6 of $\bar{p}^3\mathrm{He}^+$, with errors of $\delta\nu/\nu \approx 0.5 - 2 \times 10^{-7}$.[18)]

5. Pulse-amplified cw lasers and an optical frequency comb

Having eliminated the collisional shift, the line width of the laser and its frequency calibration remained as the largest contributory factors to the errors on measured values of the resonant frequencies.

Only pulsed lasers can provide the megawatt-scale intensities needed here to induce the $\bar{p}\mathrm{He}^+$ transitions. However, fluctuations in their frequency and line width and the difficulty of calibrating the wide range of $\bar{p}\mathrm{He}^+$ wavelengths (from infrared to ultra-

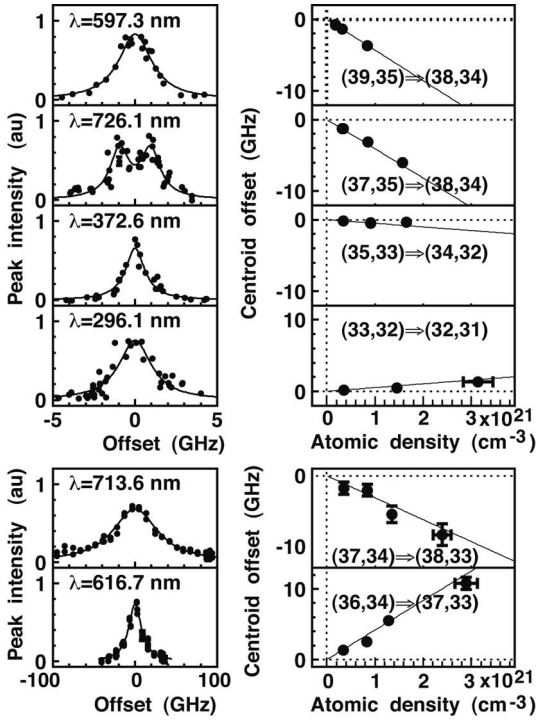

Fig. 8. (left) Antiprotonic helium laser resonance profiles: four transitions in $\bar{p}^4\mathrm{He}^+$ and two in $\bar{p}^3\mathrm{He}^+$. (right) The dependence of the transition frequencies on the helium target density. From ref. 18.

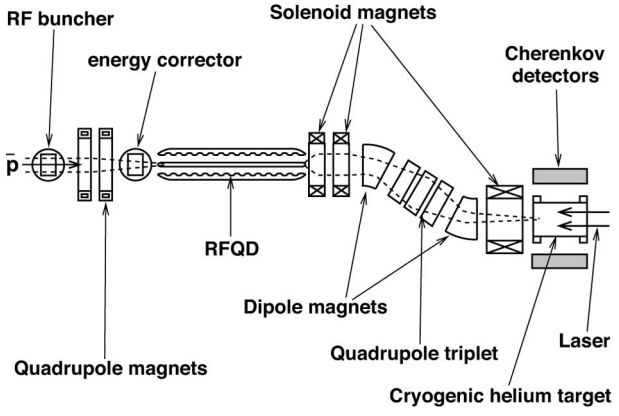

Fig. 9. Experimental layout of the radio-frequency quadrupole decelerator, and the laser spectroscopy experiment of $\bar{p}\mathrm{He}^+$. Drawing not to scale.[17)]

violet) have limited our experimental precision. We circumvented these problems by basing our experiments on a continuous-wave (cw) laser whose frequency ν_{cw} could be stabilized with a precision $<4\times10^{-10}$ against an optical comb (Fig. 10).[19)–21)] Its intensity was then amplified by a factor 10^6 to produce a pulsed laser beam of frequency $\nu_{\mathrm{pl}}\sim\nu_{\mathrm{cw}}$ with an accuracy

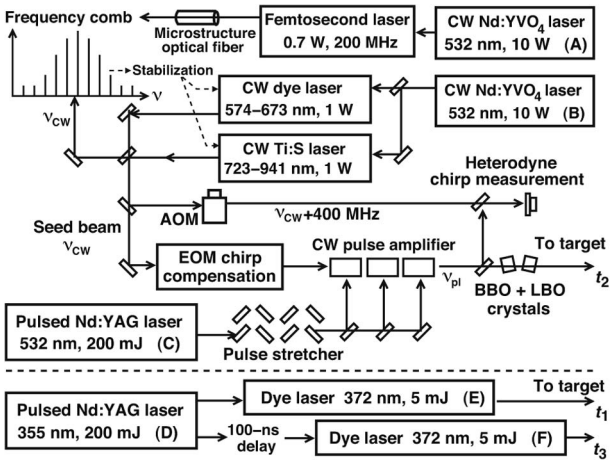

Fig. 10. Pulse-amplified cw laser stabilized against an optical frequency comb. From ref. 5.

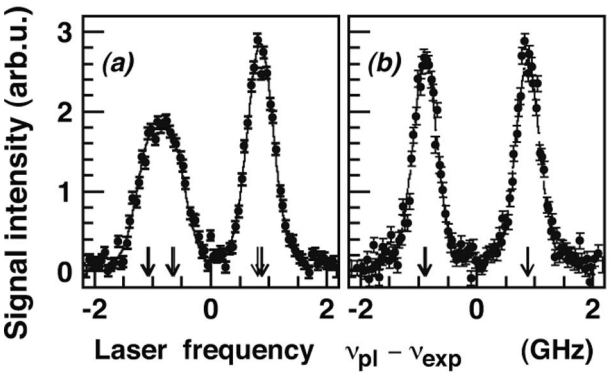

Fig. 11. Frequency profiles (laser detuning plotted against the laser-induced annihilation signal intensity of the transition (a) $(36,34)\rightarrow(37,33)$ in $\bar{p}^3\mathrm{He}^+$ and (b) $(37,35)\rightarrow(38,34)$ in $\bar{p}^4\mathrm{He}^+$.

and resolution 1–2 orders of magnitude higher than before. The profile of the $(n,\ell)=(36,34)\rightarrow(37,33)$ resonance in $\bar{p}^3\mathrm{He}^+$ is shown in Fig. 11(a). It contains

(i) eight intense lines (indicated by four arrows in Fig. 11(a), where each arrow in fact represents a closely-spaced doublet) corresponding to E1 transitions involving no spin-flip between the eight hyper-fine substates (i.e., the coupling of the electron spin, the antiproton orbital angular momentum and the antiproton spin) of states $(36,34)$ and $(37,33)$ and

(ii) 12 weak lines wherein one of the constituent particles flips its spin. Only the two peaks separated by 1.8 GHz that arise from the interaction between the orbital angular momentum of the

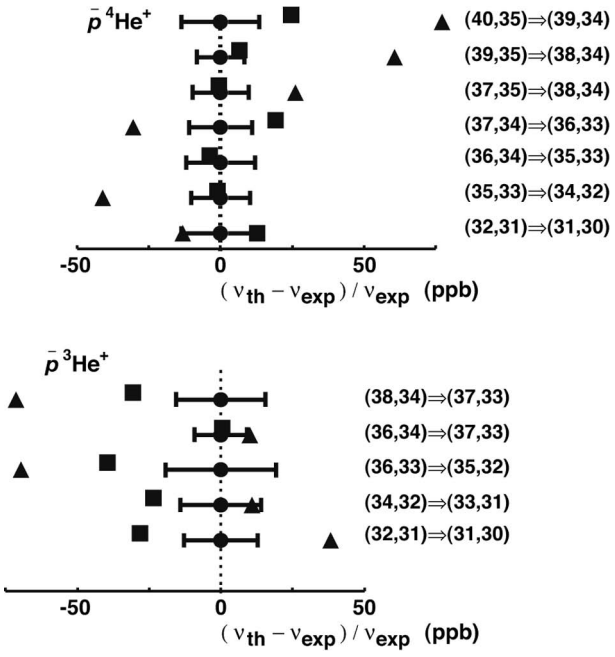

Fig. 12. Experimental $\nu_{\rm exp}$ (circles with 1σ errors) vs theoretical $\nu_{\rm th}$ (triangles[23] and squares[3]) transition frequencies. From ref. 5.

antiproton and electron spin could be resolved, however, due to the 400 MHz Doppler broadening caused by the motion of the $\bar{p}^3{\rm He}^+$ thermalized to $T = 10$ K.

The spin-averaged transition frequency $\nu_{\rm exp}$ was determined by fitting this profile with the theoretical line shape (solid line) obtained from the optical Bloch equations which describe the evolution of the $\bar{p}{\rm He}^+$ state populations during laser irradiation. The $\nu_{\rm exp}$ values of $\bar{p}^4{\rm He}^+$ resonances (Fig. 11(b)), which contain four intense, non-spin-flip lines and four weak, spin-flip ones, were similarly obtained. The ac Stark shifts caused by the laser interacting with $\bar{p}{\rm He}^+$ are estimated to be $<$MHz, due to the small scalar (-3 to 2 a.u.) and tensor ($(0.1-2)\times10^3$ a.u.) terms of the dynamic polarizability for these transitions.

6. Weighing the antiproton

The $\nu_{\rm exp}$ values thus obtained are compared with theoretical values $\nu_{\rm th}$[3),4),22),23)] (see Fig. 12), which included QED and nuclear-size ($\Delta\nu_{\rm nuc} = 2$–4 MHz) effects, and used the 2002 CODATA recommended values for fundamental constants, including $m_{\bar{p}}/m_e = m_p/m_e = 1836.15267261(85)$, $m_{^4{\rm He}}/m_e = 7294.2995363(32)$ and $m_{^3{\rm He}}/m_e = 5495.885269(11)$. Theory also provided coefficients for $d\nu_{\rm th}/d(m_p/m_e)$. These we used to determine the antiproton-to-electron mass ratio as the value $m_{\bar{p}}/m_e = 1836.152674(5)$ by minimizing the sum $\sum[\nu_{\rm th}(m_{\bar{p}}/m_e) - \nu_{\rm exp}]^2/\sigma^2_{\rm exp}$ over the 12 transitions.[5)] Here, the experimental (1σ) error $\sigma_{\rm exp} = 4$–15 MHz was the quadratic sum of the statistical (3–13 MHz) and systematic ones arising from the chirp (2–4 MHz), collisional shifts (0.1–2 MHz) and the harmonic generation (1–2 MHz). The error 5 on the last digit of $m_{\bar{p}}/m_e$ is the quadratic sum of 4 (the minimization error) and the systematic ones 3 (arising from $\sigma_{\rm syst}$) and 2 (from $\sigma_{\rm th}$). This result was included in the evaluation of the CODATA 2006 fundamental physical constants. Note that m_p, $m_{^4{\rm He}}$ and $m_{^3{\rm He}}$ are more precisely known in the atomic mass unit (u) rather than in the atomic units (au) (e.g., m_p in u was known in CODATA 2002 with a relative standard uncertainty of 1.3×10^{-10} while the proton mass in the atomic units m_p/m_e is known with a relative standard uncertainty of 4.4×10^{-10}). Our experiment therefore contributes mainly to the determination of m_p/m_e, or more precisely, m_e in the atomic mass unit.

7. *CPT* constraints on the $\bar{p}$ mass and charge

Let us now examine to what extent we can constrain the mass $m_{\bar{p}}$ and charge $Q_{\bar{p}}$ of the antiproton, if we let both $\bar{p}$ mass and charge tovary with respect to those of the proton (m_p and Q_p).

Naïvely, since the $\bar{p}{\rm He}^+$ binding energies (and hence transition frequencies) are roughly proportional to $m_{\bar{p}}Q^2_{\bar{p}}$, we expect to see a correlation between the fractional mass change $\delta m_{\bar{p}}/m_p$ vs $\delta Q_{\bar{p}}/Q_p$ such as

$$\delta m_{\bar{p}}/m_p = -2\delta Q_{\bar{p}}/Q_p.$$

The 90-%-confidence level contour in the $\delta m - \delta Q$ plane indeed shows that the *CPT* bounds on charge and mass obtained by the antiprotonic helium atoms are correlated along the $\delta m_{\bar{p}}/m_{\bar{p}} \approx -2\delta Q_{\bar{p}}/Q_{\bar{p}}$ direction, so that it is not possible to individually constrain $\delta m_{\bar{p}}/m_p$ and $\delta Q_{\bar{p}}/Q_p$. By combining the $\bar{p}{\rm He}^+$ results with the proton-to-antiproton cyclotron frequency comparison of the TRAP group at CERN LEAR,[24)] a much tighter bound on the equality of antiproton mass and charge with those of the proton of 2×10^{-9} (90-% confidence level), as shown in Fig. 13.

8. Summary and future prospects

Antiprotonic helium atoms ($\bar{p}{\rm He}^+ \equiv e^- - \bar{p} - {\rm He}^{++}$), serendipitously discovered at KEK (1991) and subsequently studied (1992–1996) at CERN's

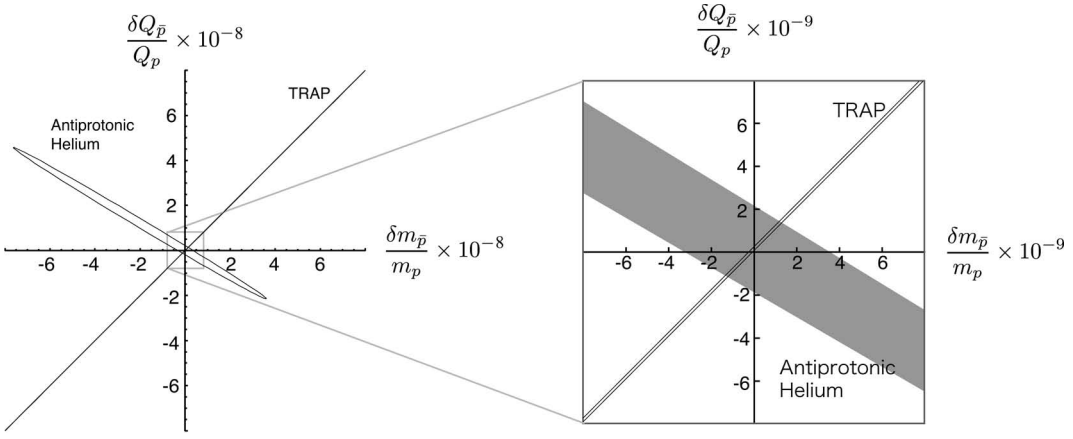

Fig. 13. A 90-%-confidence limit contour on the antiproton mass and charge deduced from the $\bar{p}\mathrm{He}^+$ laser spectroscopy is shown.

low energy antiproton ring (LEAR), have been further studied (1999–) using high-precision laser-spectroscopic methods at CERN's Antiproton Decelerator facility (AD). Experimental methods were successively developed to measure the laser transition frequencies between (n, ℓ) and $(n \pm 1, \ell - 1)$ states of $\bar{p}\mathrm{He}^+$ ($n \sim 40$ and $\ell \lesssim n-1$ are the principal and orbital quantum numbers of the antiproton) to progressively higher precisions, from the initial LEAR value of 3 parts in 10^6, to the most recent value of 9 parts in 10^9.

The first major advance was brought about by using of pulsed beams of antiprotons in high precision measurements of the $\bar{p}\mathrm{He}^+$ transition frequencies. Under this new experiment mode, a single laser pulse of high spectral purity induce transitions in $\sim 10^3$–10^4 $\bar{p}\mathrm{He}^+$ atoms simultaneously. This allowed large numbers of $\bar{p}\mathrm{He}^+$ to be produced and studied at a higher rate and precision than was possible using continuous antiproton beams. The next advance was introduced by the construction of the radio-frequency quadrupole decelerator (RFQD), a post-decelerator to the AD. The RFQD made it possible to stop antiprotons in a helium gas target at very low densities of $\rho \sim 10^{17}$ cm^{-3}, some 10^4 times lower than those previously used, and to study $\bar{p}\mathrm{He}^+$ atoms under near-vacuum conditions. This eliminated the need for the zero-density extrapolation, a large source of errors in previous measurements, thereby improving the experimental precision by nearly an order of magnitude. Another order of magnitude improvement was recently achieved by using a femtosecond optical frequency comb and continuous-wave pulse-amplified laser. The new laser system made it possible to reduce systematic uncertainties in absolute frequency determination to a few-MHz level, better than the statistical uncertainties of 3–13 MHz.

This progress in experimental technique was matched by similar advances in the theoretical methods employed in high-precision three-body QED calculations. Methods have been developed to obtain complex eigenvalues of the three-body Hamiltonian to 1-MHz-scale precisions, and QED corrections have been applied up to the order of α^5.

Comparisons of experimental ν_{exp} and theoretical ν_{th} frequencies for twelve transitions, seven in $\bar{p}^4\mathrm{He}^+$ and five in $\bar{p}^3\mathrm{He}^+$, yielded an antiproton-to-electron mass ratio of $m_{\bar{p}}/m_e = 1826.152674(5)$, which agrees with the known proton-to-electron mass ratio at the level of $\sim 2 \times 10^{-9}$. The experiment also set a limit on any CPT-violating difference between the antiproton and proton charges and masses, $(Q_p - |Q_{\bar{p}}|)/Q_p \sim (m_p - m_{\bar{p}})/m_p < 2 \times 10^{-9}$ to a 90% confidence level. If on the other hand we assume the validity of CPT invariance, the $m_{\bar{p}}/m_e$ result can be taken to be equal to m_p/m_e. The present result has in fact contributed to the improvement of the relative standard uncertainty in the proton-electron mass ratio from 0.46 ppb (2002 CODATA values)[25] to 0.43 ppb (2006 CODATA values).[6]

Further improvements in the experimental precision would be possible if the thermal Doppler broadening could be reduced. In 2007, we succeeded to achieve a higher frequency precision by performing a two-photon $(36, 34) \rightarrow (34, 32)$ resonance (by using two counter-propagating beams of $\lambda_1 \approx 372$ nm and $\lambda_2 \approx 417$ nm), which canceled the first order Doppler

width. A preliminary analysis shows that m_p/m_e can be measured with a sub-ppb ($<10^{-9}$) precision (frequency precision of $\approx$1 MHz) using this method.

In order to further improve, the use of pulsed lasers must be abandoned. So far, in order to induce strong-enough transitions for the very dilute antiprotonic helium atoms, the use of MW-class pulsed lasers has been inevitable. However, such pulsed lasers have inherent problems of frequency chirp and ac Stark shift, which are now the main source of systematic errors at the level of $\approx$1 MHz. We have therefore commenced the development of a new Doppler-free spectroscopy method using cw lasers. If our attempts succeed, it should be possible to improve the frequency precision by more than a factor 10.

However, in order to achieve a better determination of $m_{\bar{p}}/m_e$, we also need improved theoretical predictions. We now rely heavily on Korobov's calculated values which claim to have frequency precisions of $\sim$1 MHz for most of the transitions, but we need at least two theoretical predictions which agree with each other within quoted numerical errors. If both experiment and theory are improved, it appears possible to determine $m_{\bar{p}}/m_e$ as good as or even better than m_p/m_e, and to contribute to the better determination of a fundamental constant.

Acknowledgments

The author thanks ASACUSA collaborators, Drs. Masaki Hori, Eberhard Widmann and Dezső Horváth in particular, and MEXT, Japan (grant no. 20002003 and GCOE for Phys. Sci. Frontier) for support.

References

1) Yamazaki, T., Morita, N., Hayano, R.S., Widmann, E. and Eades, J. (2002) Antiprotonic helium. Phys. Rep. **366**, 183–329.
2) Hayano, R.S., Hori, M., Horváth, D. and Widmann, E. (2007) Antiprotonic helium and CPT invariance. Rep. Prog. Phy. **70**, 1995–2065.
3) Korobov, V.I. (2005) Precise spectroscopy of antiprotonic helium and sensitivity of transitions to the antiproton mass. *In* Proc. of EXA05 (eds. Hirtl, A., Marton, J., Widmann, E. and Zmeskal, J.). Austrian Academy of Sciences Press, Vienna, pp. 391–400.
4) Korobov, V.I. (2006) Hyperfine structure of metastable states in $\bar{p}^3$He$^+$ atom. Phys. Rev. A **73**, 022509-1–4.
5) Hori, M., Dax, A., Eades, J., Gomikawa, K., Hayano, R.S., Ono, N. *et al.* (2006) Determination of the antiproton-to-electron mass ratio by precision laser spectroscopy of $\bar{p}$He$^+$. Phys. Rev. Lett. **96**, 243401-1–4.
6) Mohr, P.J., Taylor, B.N. and Newell, D.B. (2009) CODATA recommended values of the fundamental physical constants: 2006. Rev. Mod. Phys. **80**, 633–730.
7) Hayano, R.S., Ishikawa, T., Iwasaki, M., Outa, H., Takada, E., Tamura, H. *et al.* (1989) Evidence for a bound-state of the $^4_\Sigma$He Hypernucleus. Phy. Let. B **231**, 355–358.
8) Yamazaki, T., Aoki, M., Iwasaki, M., Hayano, R.S., Ishikawa, T., Outa, H. *et al.* (1989) Trapping of negative kaons by metastable states during the atomic cascade in liquid helium. Phys. Rev. Lett. **63**, 1590–1592.
9) Nakamura, S.N., Iwasaki, M., Outa, H., Hayano, R.S., Watanabe, Y., Nagae, T. *et al.* (1992) Negative-pion trapping by a metastable state in liquid helium. Phys. Rev. A **45**, 6202–6208.
10) Iwasaki, M., Nakamura, S.N., Shigaki, K., Shimizu, Y., Tamura, H., Ishikawa, T. *et al.* (1991) Discovery of antiproton trapping by long-lived metastable states in liquid helium. Phys. Rev. Lett. **67**, 1246–1249.
11) Condo, G.T. (1964) On the absorption of negative pions by liquid helium. Phys. Lett. **9**, 65–66.
12) Russell, J.E. (1969) Metastable States of $\alpha\pi^-e^-$, αK^-e^-, and $\alpha\bar{p}e^-$ Atoms. Phys. Rev. Lett. **23**, 63–64.
13) Morita, N., Kumakura, M,, Yamazaki, T., Widmann, E., Masuda, H., Sugai, I. *et al.* (1994) First observation of laser-induced resonant annihilation in metastable antiprotonic helium-atoms. Phys. Rev. Lett. **72**, 1180–1183.
14) Torii, H.A., Hayano, R.S., Hori, M., Ishikawa, T., Morita, N., Kumakura, M. *et al.* (1999) Laser measurements of the density shifts of resonance lines in antiprotonic helium atoms and stringent constraint on the antiproton charge and mass. Phys. Rev. A **59**, 223–229.
15) Hori, M., Eades, J., Hayano, R.S., Ishikawa, T., Sakaguchi, J., Widmann, E. *et al.* (2001) Sub-ppm laser spectroscopy of antiprotonic helium and a CPT-violation limit on the antiprotonic charge and mass. Phys. Rev. Lett. **87**, 093401-1–4.
16) Hori, M., Eades, J., Widmann, E., Yamazaki, T., Hayano, R.S., Ishikawa, T. *et al.* (2004) Populations and lifetimes in the $v = n - \ell - 1 = 2$ and 3 metastable cascades of $\bar{p}$He$^+$ measured by pulsed and continuous antiproton beams. Phys. Rev. A **70**, 012504-1–16.
17) Lombardi, A.M., Pirkl, W. and Bylinsky, Y. (2003) First operating experience with the CERN decelerating RFQ for antiprotons. *In* Proceedings of the 2001 Particle Accelerator Conference, Chicago, 2001, EEE, Piscataway, NJ, pp. 585–587.
18) Hori, M., Eades, J., Hayano, R.S., Ishikawa, T., Pirkl, W., Widmann, E. *et al.* (2003) Direct measurement of transition frequencies in isolated $\bar{p}$He$^+$ atoms, and new *CPT*-violation limits on the antiproton charge and mass. Phys. Rev. Lett. **91**, 123401-1–4.
19) Udem, T., Holzwarth, R. and Hänsch, T.W. (2002) Optical frequency metrology. Nature, **416**, 233–237.

20) Holzwarth, R., Udem, T., Hänsch, T.W., Knight, J.C., Wadsworth, W.J. and Russell, P.S.J. (2000) Optical frequency synthesizer for precision spectroscopy. Phys. Rev. Lett. **85**, 2264–2267.
21) Jones, D.J., Diddams, S.A., Ranka, J.K., Stentz, A., Windeler, R.S., Hall J.L. *et al.* (2000) Carrier-envelope phase control of femtosecond mode-locked lasers and direct optical frequency synthesis. Science **288**, 635–639.
22) Korobov, V.I. (2003) Metastable states in the antiprotonic helium atom decaying via Auger transitions. Phys. Rev. A **67**, 062501-1–7.
23) Kino, Y., Kudo, H. and Kamimura, M. (2003) High-precision coulomb three-body calculation of antiprotonic helium atoms. Mod. Phys. Lett. A **18**, 388–397.
24) Gabrielse, G., Khabbaz, A., Hall, D.S., Heimann, C., Kalinowsky, H. and Jhe, W. (1999): Precision mass spectroscopy of the antiproton and proton using simultaneously trapped particles. Phys. Rev. Lett. **82**, 3198–3201.
25) Mohr, P.J. and Taylor, B.N. (2005) CODATA recommended values of the fundamental physical constants: 2002. Rev. Mod. Phys. **77**, 1–107.

(Received Sep. 30, 2009; accepted Nov. 17, 2009)

Profile

Ryugo Hayano is professor of experimental nuclear physics. His research concerns fundamental symmetries and interactions of nature using the spectroscopy of exotic atoms and exotic nuclei. He was born in 1952, and earned his Ph.D from the University of Tokyo in 1979. His thesis work was on the study of spin fluctuations of itinerant electrons in MnSi probed by a novel method of zero-field muon spin relaxation which he invented. He held professorship at the National Laboratory for High Energy Physics (KEK) before returning to Tokyo in 1986, where he was appointed an associate professor of nuclear physics. He was then promoted to full professor in 1997. In 1998 he received the Inoue Science Award for the discovery of Sigma hypernuclei and antiprotonic helium, and in 2008 he received the Nishina Memorial Prize, the most prestigious physics prize in Japan, for the study of antiprotonic helium atoms. He is the spokesperson of ASACUSA collaboration at CERN's antiproton decelerator facility, where he has pioneered the precision studies of antimatter using antiprotonic helium and antihydrogen.